Research Article Vol. 12, No. 9 / 1 Sep 2022 / Optical Materials Express 3749
Optical Materials EXPRESS

Spectroscopy of solid-solution transparent sesquioxide laser ceramic Tm:$LuYO_3$

Kirill Eremeev,[1] Pavel Loiko,[1] Alain Braud,[1] Patrice Camy,[1] Jian Zhang,[2] Xiaodong Xu,[3] Yongguang Zhao,[3] Peng Liu,[3] Stanislav Balabanov,[4] Elena Dunina,[5] Alexey Kornienko,[5] Liudmila Fomicheva,[6] Xavier Mateos,[7] Uwe Griebner,[8] Valentin Petrov,[8] Li Wang,[8] and Weidong Chen[8,9,*]

[1]*Centre de Recherche sur les Ions, les Matériaux et la Photonique (CIMAP), UMR 6252 CEA-CNRS-ENSICAEN, Université de Caen, 6 Boulevard du Maréchal Juin, 14050 Caen Cedex 4, France*
[2]*Key Laboratory of Transparent and Opto-Functional Inorganic Materials, Shanghai Institute of Ceramics, Chinese Academy of Sciences, 201800 Shanghai, China*
[3]*Jiangsu Key Laboratory of Advanced Laser Materials and Devices, Jiangsu Normal University, 221116 Xuzhou, China*
[4]*G. G. Devyatykh Institute of Chemistry of High-Purity Substances of the Russian Academy of Sciences, 603951 Nizhny Novgorod, Russia*
[5]*Vitebsk State Technological University, 72 Moskovskaya Ave., 210035 Vitebsk, Belarus*
[6]*Belarusian State University of Informatics and Radioelectronics, 6 Brovka St., 220027, Minsk, Belarus*
[7]*Universitat Rovira i Virgili, URV, Física i Cristal·lografia de Materials, (FiCMA)- Marcel·lí Domingo 1, 43007 Tarragona, Spain*
[8]*Max Born Institute for Nonlinear Optics and Short Pulse Spectroscopy, Max-Born-Str. 2a, D-12489 Berlin, Germany*
[9]*Fujian Institute of Research on the Structure of Matter, Chinese Academy of Sciences, 350002 Fuzhou, China*
[*]*chenweidong@fjirsm.ac.cn*

Abstract: We report on a detailed spectroscopic study of a Tm^{3+}-doped transparent sesquioxide ceramic based on a solid-solution (lutetia – yttria, $LuYO_3$) composition. The ceramic was fabricated using commercial oxide powders by hot isostatic pressing at 1600°C for 3 h at 190 MPa argon pressure. The most intense Raman peak in Tm:$LuYO_3$ at 385.4 cm^{-1} takes an intermediate position between those for the parent compounds and is notably broadened (linewidth: 12.8 cm^{-1}). The transition intensities of Tm^{3+} ions were calculated using the Judd-Ofelt theory; the intensity parameters are $\Omega_2 = 2.537$, $\Omega_4 = 1.156$ and $\Omega_6 = 0.939$ [10^{20} cm^2]. For the $^3F_4 \rightarrow {}^3H_6$ transition, the stimulated-emission cross-section amounts to 0.27×10^{-20} cm^2 at 2059nm and the reabsorption-free luminescence lifetime is 3.47 ms (the $^3F_4$ radiative lifetime is 3.85 ± 0.1 ms). The Tm^{3+} ions in the ceramic exhibit long-wave multiphonon-assisted emission extending up to at least 2.35 µm; a phonon sideband at 2.23 µm is observed and explained by coupling between electronic transitions and the dominant Raman mode of the sesquioxides. Low temperature (12 K) spectroscopy reveals a significant inhomogeneous spectral broadening confirming formation of a substitutional solid-solution. The mixed ceramic is promising for ultrashort pulse generation at >2 µm.

1. Introduction

Rare-earth sesquioxides R_2O_3 (where R is a lanthanide, Y or Sc) represent an important class of optical materials. The most interesting form of R_2O_3 compounds is the cubic one (also called C-type, sp. gr. $Ia\bar{3}$, bixbyite structure). Cubic rare-earth sesquioxides such as Y_2O_3

#471492 https://doi.org/10.1364/OME.471492
Journal © 2022 Received 25 Jul 2022; revised 18 Aug 2022; accepted 22 Aug 2022; published 30 Aug 2022

Optical Materials EXPRESS

(yttria), Sc_2O_3 (scandia) or Lu_2O_3 (lutetia) are known as excellent host media for doping with trivalent rare-earth ions (RE^{3+}) [1]. As host matrices, they feature good thermo-mechanical and thermo-optical properties [2,3] (i.e., high thermal conductivity with weak dependence on the doping level, weak isotropic thermal expansion, small and positive dn/dT coefficient), low phonon energies (for oxide materials), and wide transparency [4]. The RE^{3+} dopant ions substitute for the host-forming R^{3+} metal cations in two types of sites (C_2 and C_{3i} symmetry) with VI-fold oxygen coordination [5,6]. However, the spectroscopic properties of RE^{3+}-doped R_2O_3 compounds are mainly determined by C_2 species (about 3/4 of ions) since for the centrosymmetric C_{3i} ones (about 1/4 of ions), the electric dipole transitions are not enabled [1]. The RE^{3+} ions in cubic sesquioxides experience strong crystal fields leading to large Stark splitting of their multiplets and, consequently, broad emission bands. The crystal-field strength increases in the series $R^{3+} = Y^{3+} \rightarrow Lu^{3+} \rightarrow Sc^{3+}$ according to the variation of the ionic radius, making it possible to alter the spectral properties by changing the host composition [7].

The main drawback of R_2O_3 crystals are their extremely high melting points (e.g., 2425°C for Y_2O_3) complicating the crystal growth. So far different techniques have been used for growing R_2O_3 crystals, such as heat exchanger growth method (HEM), micro-pulling-down (μ-PD), Czochralski (Cz), etc. [8,9]. Still, single-crystals suffer from coloration, Rhenium (Re) impurities (when using Re crucibles), and a gradient of RE^{3+} dopant concentration (especially for Sc_2O_3). During the past decades, the transparent ceramic technology emerged as a competitive approach to the single-crystal growth [10]. It offers: (i) much lower synthesis temperatures (<1800°C); (ii) easier RE^{3+} doping in terms of higher available concentrations and more uniform ion distribution; (iii) well-preserved spectroscopic and thermal properties; (iv) possibility to fabricate mixed compositions $(R_1,R_2)_2O_3$ with well-controlled R_1/R_2 ratio; and (v) size-scalability. Laser-quality RE^{3+}-doped yttria [11,12], lutetia [13,14] and scandia [15] ceramics have been developed. The main challenge for ceramics is reaching high transparency close to the theoretical limit (i.e., weak light scattering owing to residual pores, possible secondary phases at the grain boundaries, etc.).

Substitutional solid solutions $A_{1-x}B_x$ ($0 < x < 1$) also called "mixed" materials are attracting attention for tailoring the spectroscopic properties of the dopant RE^{3+} ions [16–19] as, under the condition of different crystal-field strengths associated with the parent compounds A and B, the absorption / emission lines of the dopants may experience strong inhomogeneous broadening. For cubic sesquioxides, isostructural solid-solutions with a general composition $(Y_{1-x-y}Lu_xSc_y)_2O_3$ exist in the full range of x and y. The same is true also for mixing with some active RE^{3+} ions, as long as their stoichiometric compositions (RE_2O_3) possess the same cubic symmetry, e.g. Yb, Tm, Ho or Er. Although the growth of "mixed" sesquioxide crystals has been reported [19,20], it is much easier to fabricate such compounds via a transparent ceramic technology. Recently, laser ceramics in the lutetia-scandia and lutetia-yttria binary systems were developed [16,18,21–25].

Thulium (Tm^{3+}) doped sesquioxides attract attention because of their suitability for efficient lasing around 2 μm according to the $^3F_4 \rightarrow {}^3H_6$ electronic transition [26]. Tm^{3+} ions experience strong crystal-fields in R_2O_3 compounds. The resulting substantial Stark splitting of their multiplets determines broad emission spectra naturally extending above 2 μm [7]. The latter property is of practical importance for broadly tunable and especially mode-locked lasers [27,28] as this helps to avoid the structured water vapor absorption in the atmosphere spectrally located at < 2 μm which is detrimental for achieving femtosecond pulses. Recently, femtosecond mode-locked Tm ceramic lasers based on "mixed" sesquioxides such as Tm:$(Lu,Sc)_2O_3$ and Tm:$(Lu,Y)_2O_3$ were reported [28–30].

The present work is devoted to the spectroscopic properties of Tm^{3+} ions in a "mixed" (lutetia – yttria) sesquioxide laser ceramic, with the goal of revealing the effect of compositional disorder on the inhomogeneous broadening of absorption and emission lines, in order to better understand the potential of such materials for generation of few-optical-cycle pulses.

Optical Materials EXPRESS

2. Synthesis of transparent ceramics

Commercial powders of rare-earth oxides, Lu_2O_3 (purity: 4N), Y_2O_3 (5N) and Tm_2O_3 (4N), from Jiahua Advanced Material Resources, China, were used as raw materials. They were weighed according to the composition of 3.0 at.% Tm:$(Lu_{0.5}Y_{0.5})_2O_3$. The mixed powders were ball-milled in ethanol for 24 h with 1.0 at % monoclinic ZrO_2 powder (Shandong Sinocera Functional Material, China) serving as a sintering aid. The milled slurries were dried in an oven at 70°C for 24 h and then sieved through a 100-mesh screen. After that, the powders were dry-pressed into pellets by a 12 mm-diameter mold and cold isostatically pressed at 200 MPa for 5 min. All the green bodies were calcined at 850°C for 4 h to remove the residue organics. After that, the samples were first pre-sintered at 1650°C for 4 h in vacuum under a pressure lower than 1.0×10^{-3} Pa, equipped with a tungsten mesh as the heating element. Then, the pre-sintered ceramics were treated by hot isostatic pressing (HIPing) at 1600°C for 3 h in 190 MPa argon pressure to eliminate residual pores. Finally, the HIP-treated samples were annealed at 1200°C for 24 h in a muffle furnace in air to compensate the oxygen loss during the vacuum pre-sintering and the following HIP treatment. Then, the ceramic disks were polished on both sides to laser quality level, Fig. 1. The obtained ceramic disks were transparent and slightly yellow colored due to the Tm^{3+} doping. The calculated Tm^{3+} ion density in the "mixed" ceramic was $N_{Tm} = 8.34 \times 10^{20}$ at/cm^3.

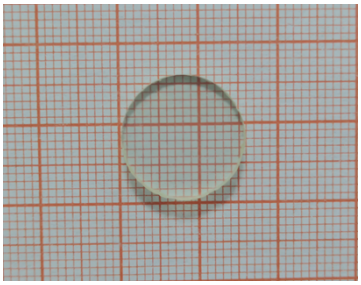

Fig. 1. A photograph of annealed and polished 3.0 at.% Tm:$LuYO_3$ ceramic disk.

To observe the microstructure of the ceramic, its polished surface was thermally etched at 1400°C for 2 h in a muffle furnace in air. The thermally etched surfaces of the 3.0 at.% Tm:$LuYO_3$ ceramics before and after HIPing were characterized using a Scanning Electron Microscope (SEM, TM3000, Hitachi, Japan). The pre-sintered ceramic has an average grain size of 1 μm and it contains sub-μm sized pores localized at the grain boundaries, Fig. 2(a). After HIPing, the mean grain size increases to 2.4 μm. The ceramic exhibits a close-packed microstructure with clean grain boundaries, Fig. 2(b).

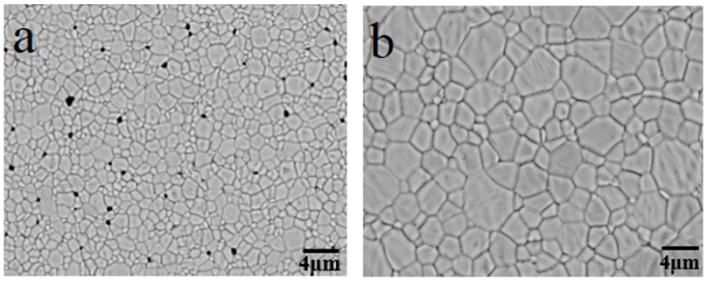

Fig. 2. SEM images of the thermally etched surface of the 3.0 at.% Tm:$LuYO_3$ ceramics: (a) a pre-sintered sample; (b) a sample after HIPing.

Optical Materials EXPRESS

For comparison, two parent ceramics, Tm:Lu_2O_3 and Tm:Y_2O_3, doped with 3 at.% Tm^{3+} ($N_{Tm} = 8.61 \times 10^{20}$ cm^{-3} and 7.85×10^{20} cm^{-3}, respectively), were fabricated.

3. Results and discussion

3.1. Raman spectra

The room temperature (RT) Raman spectra were measured using a confocal laser microscope (Renishaw inVia) equipped with a × 50 Leica objective and an Ar^+ ion laser (514 nm). For cubic sesquioxides (sp. gr. $Ia\bar{3}$) possessing a body-centered structure, the factor group analysis predicts the following irreducible representations for the optical and acoustical modes at the center of the Brillouin zone ($\boldsymbol{k} = 0$): $\Gamma_{op} = 4A_g + 4E_g + 14F_g + 5A_{2u} + 5E_u + 16F_u$ (of which 22 modes (A_g, E_g, and F_g) are Raman-active, 16 modes (F_u) are IR-active, and the rest are silent) and $\Gamma_{ac} = F_u$ [31,32].

Figure 3(a) shows the Raman spectra of the Tm^{3+}-doped $LuYO_3$, Y_2O_3 and Lu_2O_3 ceramics. They are typical for cubic (C-type) sesquioxides. The vibrational spectra exhibit two distinct frequency ranges: the relative position and intensities of the modes above 300 cm^{-1} are rather similar for different ceramic compositions indicating that they are most probably related to oxygen motions and deformations of the [AO_6] octahedrons [31]. The most intense peak is assigned to $F_g + A_g$ vibrations [31], Fig. 3(b). For the yttria and lutetia ceramics, it is centered at 377.8 and 391.4 cm^{-1}, respectively, and its linewidth is nearly the same (6.7 and 7.4 cm^{-1}, respectively). For the "mixed" ceramic, this peak takes an intermediate position (385.4 cm^{-1}) and it is notably broadened (linewidth: 12.8 cm^{-1}) confirming the formation of a substitutional solid-solution. A similar tendency is observed for other well assigned modes in the high-frequency range of ~300 – 600 cm^{-1}. The peak corresponding to the maximum phonon energy (the $F_g + A_g$ vibrations) is observed at 593 cm^{-1} (Tm:Y_2O_3), 603 cm^{-1} (Tm:$LuYO_3$) and 612 cm^{-1} (Tm:Lu_2O_3).

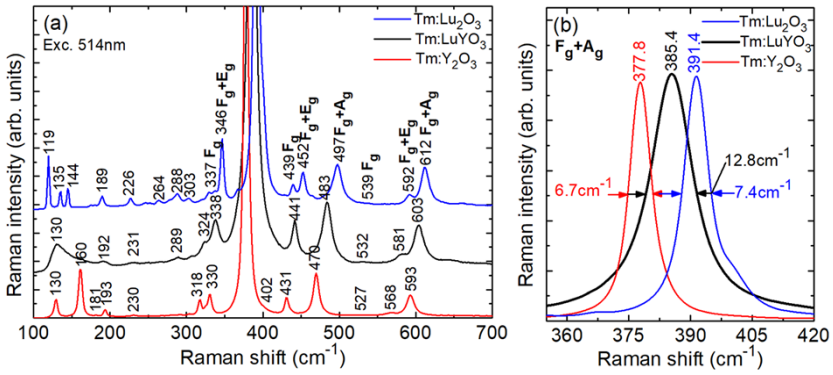

Fig. 3. Unpolarized Raman spectra of Tm^{3+}-doped Lu_2O_3, Y_2O_3 and $LuYO_3$ ceramics: (a) overview spectra; (b) a close look at the most intense mode ($F_g + A_g$), $\lambda_{exc} = 514$ nm. *Numbers* indicate the Raman frequencies in cm^{-1}.

3.2. Absorption spectra and Judd-Ofelt analysis

The transmission / absorption spectra were measured using a spectrophotometer (Lambda 1050, Perkin Elmer).

The Tm:$LuYO_3$ ceramic exhibited a relatively high linear transmission of 81.5% at 2.2 μm (out of the Tm^{3+} absorption bands), close to the theoretical limit, $T_0 = 2n/(n^2 + 1) = 82.0\%$ (a formula accounting for multiple light reflections, $n = 1.918$ is the estimated refractive index of $LuYO_3$ [33]). The absorption spectrum of Tm^{3+} ions in the "mixed" ceramic is shown in Fig. 4.

Optical Materials EXPRESS

Bands related to transitions from the ground-state ($^3H_6$) to the excited-states ranging from $^3F_4$ up to $^3P_{0-2}$ are observed. The UV absorption edge is observed at ~250 nm (for undoped Lu_2O_3, the optical bandgap E_g is 5.6 eV [34] or ~221 nm).

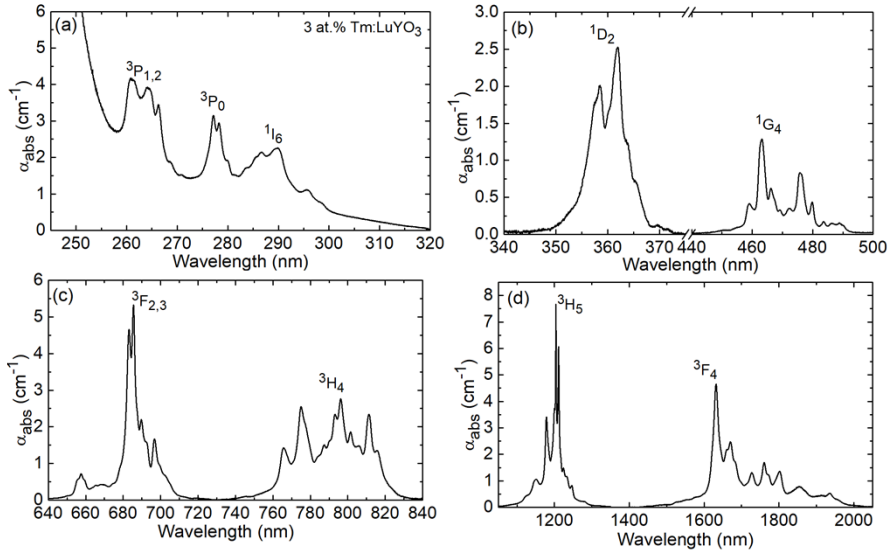

Fig. 4. RT absorption spectra of the 3 at.% Tm:$LuYO_3$ ceramic in the spectral range of (a) 245 – 320 nm, (b) 340 – 500 nm, (c) 640 – 840 nm, (d) 1050 – 2050 nm.

The absorption cross-sections σ_{abs} for the $^3H_6 \rightarrow {}^3H_4$ transition of Tm^{3+} in the "mixed" $LuYO_3$ ceramic, and in Y_2O_3 and Lu_2O_3, are shown in Fig. 5. This absorption band is suitable for pumping Tm-lasers using commercially available AlGaAs diode lasers emitting around 0.8 µm. For the "mixed" ceramic, the absorption spectrum is broadened as compared to both parent compounds; the maximum σ_{abs} is 0.33×10^{-20} cm^2 at 796.2 nm corresponding to an absorption bandwidth $\Delta\lambda_{abs}$ of ~21 nm (combining several peaks), compared with $\sigma_{abs} = 0.37 \times 10^{-20}$ cm^2 at 796.7 nm with $\Delta\lambda_{abs}$ of ~7 nm for the Tm:Y_2O_3 ceramic.

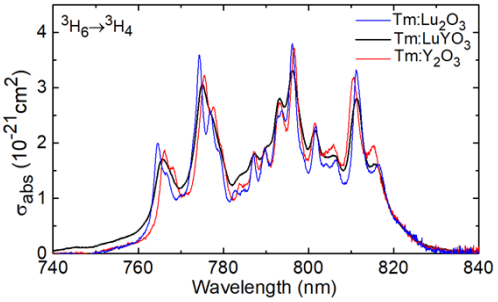

Fig. 5. Absorption cross-sections, σ_{abs}, for the $^3H_6 \rightarrow {}^3H_4$ transition of Tm^{3+} ions in the $LuYO_3$, Y_2O_3 and Lu_2O_3 ceramics.

The measured absorption spectrum was analyzed using the standard Judd-Ofelt (J-O) theory [35,36]. Eight Tm^{3+} transitions were considered. The set of reduced squared matrix elements $U^{(k)}$ was taken from [37]. The magnetic-dipole (MD) contributions to transition intensities (for transitions with $\Delta J = J - J' = 0, \pm 1$) were calculated within the Russel-Saunders approximations using the wave functions of the free Tm^{3+} ion. The refractive index of the "mixed" ceramic

Optical Materials EXPRESS

$LuYO_3$ was calculated using the dispersion curves of the parent compounds [34]. More details about the J - O analysis can be found elsewhere [38].

For calculating the absorption oscillator strengths, we have used the full Tm^{3+} ions density (N_{Tm}), although some authors suggest to account only for ions located in C_2 sites [~(3/4)N_{Tm}] [39]. However, for a "mixed" ceramic, the actual distribution of dopant ions over the C_2 and C_{3i} sites may significantly differ from that for the parent material.

Table 1 contains the experimental (f^{Σ}_{exp}) and calculated (f^{Σ}_{calc}) absorption oscillator strengths. Here, the superscript "Σ" indicates a total value (ED + MD). The root mean square (r.m.s.) deviation between the f^{Σ}_{exp} and f^{Σ}_{calc} values is $\delta_{rms} = 1.202$, mainly due to the transitions to thermally coupled levels $^3F_2 + {}^3F_3$ and $^1I_6 + {}^3P_0 + {}^3P_1$. For the lowest-lying excited-state ($^3F_4$), a relatively good agreement is observed. The corresponding J - O parameters are $\Omega_2 = 2.537$, $\Omega_4 = 1.156$ and $\Omega_6 = 0.939$ [10^{20} cm^2]. These values agree well with those reported recently for another Tm^{3+}-doped "mixed" sesquioxide ceramic with a composition $(Lu,Sc)_2O_3$, $\Omega_2 = 2.429$, $\Omega_4 = 1.078$ and $\Omega_6 = 0.653$ [10^{20} cm^2] [16].

Table 1. Experimental and Calculated Absorption Oscillator Strengths[a] for Tm^{3+} Ions in $LuYO_3$[a]

Transition	$\langle\lambda_{abs}\rangle$, nm	$\langle E\rangle$, cm^{-1}	$\langle n\rangle$	Γ, cm^{-1}nm	$f^{\Sigma}_{exp}\times10^6$	$f^{\Sigma}_{calc}\times10^6$
$^3H_6\rightarrow{}^3F_4$	1763	5672	1.912	444.25	2.038	2.126^{ED}
$^3H_6\rightarrow{}^3H_5$	1206	8292	1.921	243.02	2.308	$1.458^{ED}+0.530^{MD}$
$^3H_6\rightarrow{}^3H_4$	795	12585	1.933	101.29	2.192	2.562^{ED}
$^3H_6\rightarrow{}^3F_2+{}^3F_3$	684	14616	1.939	68.308	1.977	3.216^{ED}
$^3H_6\rightarrow{}^1G_4$	473	21155	1.964	14.359	0.881	0.753^{ED}
$^3H_6\rightarrow{}^1D_2$	361	27738	2.009	20.231	2.117	2.114^{ED}
$^3H_6\rightarrow{}^1I_6+{}^3P_0+{}^3P_1$	284	35178	2.084	24.788	4.131	$1.778^{ED}+0.029^{MD}$
$^3H_6\rightarrow{}^3P_2$	263	37968	2.126	13.235	2.585	2.411^{ED}
δ_{rms}						*1.202*

[a] $\langle\lambda_{abs}\rangle$ - "center of gravity" of the absorption band, $\langle E\rangle$ - energy barycenter of the multiplet, $\langle n\rangle$ - mean refractive index, Γ – integrated absorption coefficient, f^{Σ}_{exp} and f^{Σ}_{calc} – experimental and calculated absorption oscillator strengths, respectively, ED and MD – electric and magnetic dipole, respectively.

Using the determined J - O parameters, the probabilities (ED + MD) of spontaneous radiative transitions for particular emission channels J → J' $A_{\Sigma}{}^{calc}$(JJ'), the total probabilities of radiative transitions from excited-states $A_{tot} = \Sigma_{J'}A_{\Sigma}{}^{calc}$(JJ'), the luminescence branching ratios B(JJ') = $A_{\Sigma}{}^{calc}$(JJ')/A_{tot} and the radiative lifetimes $\tau_{rad} = 1/A_{tot}$ were calculated, cf. Table 2. The mean emission wavelengths $\langle\lambda_{em}\rangle$ were estimated using the barycenter energies of Tm^{3+} multiplets $\langle E\rangle$ from Table 1. For the $^3F_4$ and $^3H_4$ states, τ_{rad} amounts to 4.18 ms and 0.61 ms, respectively.

3.3. Emission (spectra and lifetimes)

The Tm^{3+} luminescence was excited at ~796 nm using a CW Ti:Sapphire laser and the spectra were measured using an optical spectrum analyzer (OSA, AQ6376, Yokogawa) and a ZrF_4 fiber. The spectral sensitivity of the set-up was calibrated using a 20 W quartz iodine lamp.

The normalized RT emission spectra of Tm^{3+} ions in the $LuYO_3$, Y_2O_3 and Lu_2O_3 ceramics are shown in Fig. 6(a). The observed emission is related to the $^3F_4 \rightarrow {}^3H_6$ transition. The spectra are very broad spanning from 1.6 up to 2.35 μm. For the "mixed" ceramic, the spectrum exhibits a notable inhomogeneous broadening as compared to those of the parent compounds. The spectral maximum is found at ~1936nm. For the quasi-three-level $^3F_4 \rightarrow {}^3H_6$ Tm^{3+} laser, emission is expected at the long-wave wing of the luminescence spectrum. For Tm^{3+}-doped cubic sesquioxides, a broad peak above 2 μm is observed where maximum laser gain will occur.

Optical Materials EXPRESS

Table 2. Calculated Emission Probabilities for Tm^{3+} Ions in $LuYO_3$[a]

Excited state	Terminal state	$\langle\lambda_{em}\rangle$, nm	A_Σ^{calc}(JJ'), s^{-1}	B(JJ'), %	A_{tot}, s^{-1}	τ_{rad}, ms
$^3F_4$	$^3H_6$	1763.0	239.36^{ED}	100	239.36	4.178
$^3H_5$	$^3F_4$	3816.8	$9.69^{ED} + 0.26^{MD}$	2.5	406.09	2.463
	$^3H_6$	1206.0	$291.03^{ED} + 105.11^{MD}$	97.5		
$^3H_4$	$^3H_5$	2329.4	$25.20^{ED} + 10.48^{MD}$	2.2	1649.19	0.606
	$^3F_4$	1446.5	$122.23^{ED} + 27.27^{MD}$	9.1		
	$^3H_6$	794.6	1464.01^{ED}	88.7		
$^3F_2$+$^3F_3$	$^3H_4$	4923.7	$20.48^{ED} + 0.39^{MD}$	0.4	4898.36	0.204
	$^3H_5$	1581.3	590.23^{ED}	12.0		
	$^3F_4$	1118.1	$818.81^{ED} + 72.33^{MD}$	18.2		
	$^3H_6$	684.2	3396.12^{ED}	69.4		
$^1G_4$	$^3F_2 + ^3F_3$	1529.3	$86.00^{ED} + 4.64^{MD}$	3.1	2867.78	0.349
	$^3H_4$	1166.9	$257.70^{ED} + 39.56^{MD}$	10.4		
	$^3H_5$	777.4	$845.70^{ED} + 161.92^{MD}$	35.1		
	$^3F_4$	645.9	$215.47^{ED} + 13.49^{MD}$	8.0		
	$^3H_6$	472.7	1243.3^{ED}	43.4		
$^1D_2$	$^1G_4$	1519.1	188.17^{ED}	3.7	34688.5	0.029
	$^3F_2 + ^3F_3$	762.1	$2320.43^{ED} + 185.66^{MD}$	4.0		
	$^3H_4$	659.9	2010.27^{ED}	5.8		
	$^3H_5$	514.2	135.03^{ED}	0.4		
	$^3F_4$	453.2	18445.5	53.2		
	$^3H_6$	360.5	11403.4	32.9		

[a] $\langle\lambda_{em}\rangle$ - mean emission wavelength, A_Σ^{calc}(JJ') - probability of spontaneous transitions, B(JJ') - luminescence branching ratio, A_{tot} - total probability of spontaneous transitions from an excited-state, τ_{rad} – radiative lifetime.

For the Tm:$LuYO_3$ ceramic, it is centered at 2058 nm, in between the positions for Tm:Y_2O_3 (2049 nm) and Tm:Lu_2O_3 (2063 nm). The emission bandwidth for this peak also exceeds those for the parent compounds supporting our assumption about the formation of a solid-solution.

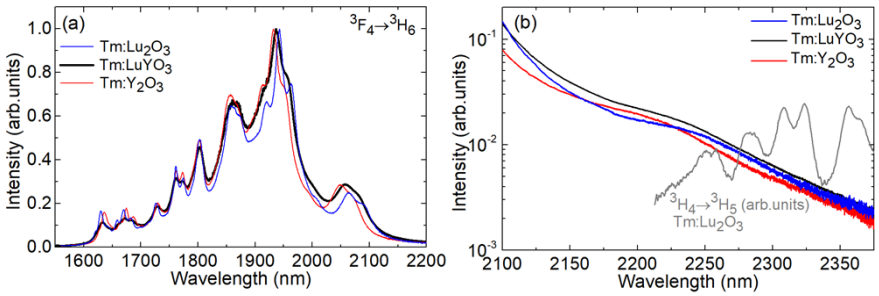

Fig. 6. (a,b) RT luminescence spectra of Tm:$LuYO_3$, Tm:Y_2O_3 and Tm:Lu_2O_3 ceramics around 2 µm: (a) overview of the spectra, (b) a close look at the 2100 – 2375 nm range, semi-log scale, *grey curve* – emission spectrum for the $^3H_4 \rightarrow ^3H_5$ Tm^{3+} transition in a low-doped (<0.1 at.%) Tm:Lu_2O_3 shown for comparison. λ_{exc} = 796 nm.

A careful examination of the long-wave part of the luminescence spectra of all the studied ceramics indicates that their emission extends up to at least 2.35 µm (further measurement

Optical Materials EXPRESS

was limited by the sensitivity of our set-up). It is associated with the $^3F_4 \rightarrow {}^3H_6$ transition of Tm^{3+} according to the luminescence decay studies: the luminescence lifetime remains nearly constant when changing the detection wavelength between 1.8 – 2.3 μm. One may argue that such long-wave emission may also partially originate from the $^3H_4 \rightarrow {}^3H_5$ electronic transition [40]. However, no characteristic spectral features of this transition are found in the spectra. To prove this, we have used a low-doped (<0.1 at.%) Tm:Lu_2O_3 crystal exhibiting almost no self-quenching of the $^3H_4$ lifetime to measure the luminescence spectrum of the $^3H_4 \rightarrow {}^3H_5$ transition, Fig. 6(b). It reveals several well-resolved emission peaks centered at 2282, 2308, 2324 and 2356 nm which are not found in the spectra of the ceramics. In contrast, the long-wave part of the emission spectrum of the ceramics is almost structureless and follows an exponential law at >2.25 μm, as seen from Fig. 6(b) plotted in a semi-log scale.

The long-wave limit for purely electronic transitions $^3F_4 \rightarrow {}^3H_6$ is determined by the crystal-field splitting of the involved multiplets and, in particular, by the energy gap between the lowest sub-level of the $^3F_4$ state (5643 cm^{-1}, Y_1) and the highest sub-level of the $^3H_6$ ground-state (810 cm^{-1}, Z_{13}, see below) [41]. This yields a value of 2069 nm. All the emissions above this wavelength are multiphonon-assisted (or vibronic) as they are related to the coupling between electrons and host vibrations (phonons) [42].

The very broad peak centered at 2.23 μm (for Tm:$LuYO_3$) is interpreted as a phonon sideband, see [42,43] for this term. Note that it takes an intermediate position between those for Tm:Y_2O_3 (2.21 μm) and Tm:Lu_2O_3 (2.25 μm) which agrees with the difference in the crystal-field strengths. This indicates that the position of this peak could be linked to those of electronic transitions. Indeed, for the "mixed" ceramic, the energy gap between the prominent electronic emission band centered at 2058nm and the above-described sideband (2236 nm) is ~387 cm^{-1}. This well matches the most intense Raman peak of this material corresponding to vibration with an energy $h\nu_{ph} = 385.4\,cm^{-1}$, Fig. 3(b). Thus, one can describe the appearance of the phonon sideband in the Tm^{3+} emission spectrum as transitions to a virtual energy level located slightly above the highest electronic sub-levels of the $^3H_6$ multiplet [44], i.e., having an energy $E(Z_{13}) + h\nu_{ph}$.

The stimulated-emission (SE) cross-sections, σ_{SE}, for the $^3F_4 \rightarrow {}^3H_6$ transition of Tm^{3+} ions in the $LuYO_3$ ceramic were calculated using two methods, namely, (i) the reciprocity method [45], and (ii) the Füchtbauer – Ladenburg (F-L) formula [46]. The σ_{SE} spectra obtained by both methods were in good agreement with each other, considering the effect of reabsorption on the measured emission spectrum. In the F-L formula, we have used a radiative lifetime of the $^3F_4$ state $\tau_{rad} = 3.85 \pm 0.1$ ms to fit the two methods which reasonably agrees with that determined using the J - O theory (4.18 ms). In Fig. 7(a), the combined SE cross-section spectrum is shown. The maximum σ_{SE} is 0.75×10^{-20} cm^2 at 1937 nm and at longer wavelengths where the laser operation is expected, $\sigma_{SE} = 0.27 \times 10^{-20}$ cm^2 at 2059 nm.

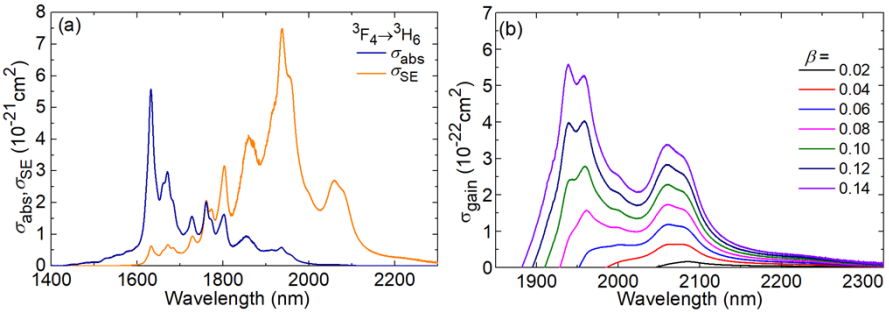

Fig. 7. The $^3H_6 \leftrightarrow {}^3F_4$ transition of Tm^{3+} ions in the $LuYO_3$ ceramic: (a) absorption, σ_{abs}, and stimulated-emission (SE), σ_{SE}, cross-sections; (b) the gain cross-sections, $\sigma_{gain} = \beta\sigma_{SE} - (1 - \beta)\sigma_{abs}$, for different inversion ratios $\beta = N_2(^3F_4)/N_{Tm}$.

Optical Materials EXPRESS

The $^3F_4 \rightarrow {}^3H_6$ transition of Tm^{3+} ions represents a quasi-three-level laser scheme with reabsorption at the laser wavelength. Thus, the gain cross-sections, $\sigma_{gain} = \beta\sigma_{SE} - (1-\beta)\sigma_{abs}$, are calculated, where $\beta = N_2(^3F_4)/N_{Tm}$ is the population inversion ratio. The gain profiles of the "mixed" ceramic are shown in Fig. 7(b). The spectra are smooth and broad extending until 2.35 µm. For small inversion ratios ($\beta < 0.10$), two local maxima appear in the spectra, centered at ~2085 and 2059nm. For $\beta = 0.04$, the gain bandwidth (FWHM) is as broad as 75 nm. For higher $\beta > 0.10$, the gain maxima experience a blue-shift to ~1960 and 1938nm. The observed broadband gain properties indicate the high suitability of this ceramic for generation of sub-100 fs pulses.

The existence of gain at long wavelengths well above 2.1 µm due to the multiphonon-assisted transitions is an important prerequisite for generation of ultrashort pulses from mode-locked Tm sesquioxide lasers. Indeed, the emission spectra of such lasers delivering pulses in the sub-100 fs time domain contained spectral components extending up to 2.3 µm [30,47].

The luminescence dynamics was studied using a ns optical parametric oscillator (Horizon, Continuum), a 1/4 m monochomator (Oriel 77200), an InGaAs detector and an 8 GHz digital oscilloscope (DSA70804B, Tektronix). To avoid the effect of reabsorption (radiation trapping) on the measured lifetimes, finely powdered samples were used.

For the $^3F_4$ Tm^{3+} state, the decay curves are well described by a single-exponential law, Fig. 8(a), yielding $\tau_{lum} = 3.470$ ms for the Tm:$LuYO_3$ ceramic. This value is slightly longer compared to the parent compounds, 3.224 ms (Tm:Lu_2O_3) and 2.919 ms (Tm:Y_2O_3). Note that the measured luminescence lifetimes of the $^3F_4$ state for the studied sesquioxide ceramics are close to those obtained for single-crystals with low Tm^{3+} doping levels (<0.3 at.%), i.e., 3.38 ms (Tm:Lu_2O_3) and 3.54 ms (Tm:Y_2O_3) [7], indicating a relatively weak concentration quenching.

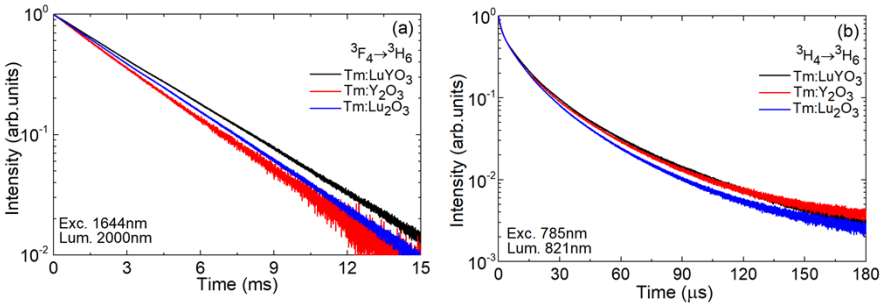

Fig. 8. RT luminescence decay curves for Tm^{3+} ions in the $LuYO_3$, Y_2O_3, and Lu_2O_3 ceramics: (a) decay from the $^3F_4$ state, $\lambda_{exc} = 1644$ nm, $\lambda_{lum} = 2000$nm; (b) decay from the $^3H_4$ state, $\lambda_{exc} = 785$ nm, $\lambda_{lum} = 821$ nm. Powdered samples.

For the $^3H_4$ pump level, the decay is clearly not single-exponential, Fig. 8(b), owing to the efficient cross-relaxation (CR) process, $^3H_4 + {}^3H_6 \rightarrow {}^3F_4 + {}^3F_4$. For the Tm:$LuYO_3$ ceramics, the mean luminescence lifetime of the $^3H_4$ state $<\tau_{lum}>$ is only 24 µs. It is much shorter than the so-called intrinsic lifetime (measured at a very low Tm^{3+} doping level, i.e., unaffected by the CR process), $\tau_{lum,0} = 350$ µs for Tm:Lu_2O_3 [7]. Thus, the estimated CR rate, $W_{CR} = (1/\tau_{lum}) - (1/\tau_{lum,0})$, is about 3.88×10^4 s^{-1} (for 3 at.% Tm^{3+} doping). The CR rate is quadratically proportional to the doping concentration, $W_{CR} = C_{CR}(N_{Tm})^2$ [48], where $C_{CR} = 0.56 \times 10^{-37}$ $cm^6 s^{-1}$ is the concentration-independent CR parameter.

Table 3 summarizes the measured luminescence lifetimes.

Optical Materials EXPRESS

Table 3. Measured Luminescence Lifetimes of the $^3F_4$ and $^3H_4$ Tm^{3+} States in the $LuYO_3$, Y_2O_3 and Lu_2O_3 Ceramics

Ceramic	τ_{lum}, ms	
	$^3H_4$	$^3F_4$
$LuYO_3$	0.024	3.470
Y_2O_3	0.025	2.919
Lu_2O_3	0.022	3.224

3.4. Low-temperature spectroscopy

For low temperature (LT, 12 K) studies, the samples were mounted in an APD DE-202 closed-cycle cryo-cooler equipped with an APD HC 2 Helium vacuum cryo-compressor and a Laceshore 330 temperature controller.

The $^3H_6 \rightarrow {}^3F_4$ (absorption) and $^3F_4 \rightarrow {}^3H_6$ (luminescence) Tm^{3+} transitions were considered giving access to the crystal-field splitting of both multiplets. In Fig. 9, the obtained LT absorption spectra are plotted vs. the photon energy and the LT emission spectra – vs. (E_{ZPL} – photon energy). The considered transitions are of pure ED nature and thus no signatures of C_{3i} sites could be observed. For the RE^{3+} ions in C_2 sites, each multiplet $^{2S+1}L_J$ with an integer J is split into a total of 2J + 1 sub-levels. A careful examination of the LT spectra of the parent compounds allowed us to determine the full set of Stark sub-levels for both mutiplets, cf. Table 4. Here, we use the empirical notations for the electronic levels proposed by Lupei *et al.* [49]: $^3H_6 = Z_i$ ($i = 1 \ldots 13$) and $^3F_4 = Y_j$ ($j = 1 \ldots 9$). The total Stark splitting of the ground-state, $\Delta E(^3H_6)$, increased in the R = Y $\rightarrow$ Lu series, from 788 to 828 cm^{-1}. The peaks corresponding to electronic transitions were relatively narrow and experienced a notable shift between Y_2O_3 and Lu_2O_3 according to the different crystal-field strengths in these compounds. For the most intense electronic line in absorption, designated as $Z_0 \rightarrow Y_7$, the peak positions / widths are 6112.8 / 6.1 cm^{-1} (Y_2O_3) and 6134.9 / 5.5 cm^{-1} (Lu_2O_3), respectively.

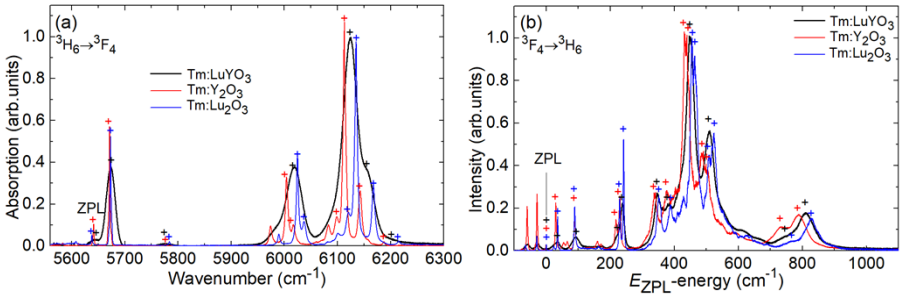

Fig. 9. Low-temperature (LT, 12 K) spectroscopy of Tm^{3+} ions in the $LuYO_3$, Y_2O_3, Lu_2O_3 ceramics: (a) absorption spectra, the $^3H_6 \rightarrow {}^3F_4$ transition; (b) luminescence spectra, the $^3F_4 \rightarrow {}^3H_6$ transition, ZPL – zero-phonon-lines, "+" indicate the assigned electronic transitions.

For the "mixed" ceramic, the LT spectroscopy does not reveal any signatures of two distinct Tm^{3+} species (e.g., the presence of two sets of electronic transitions or any dependence of the luminescence spectrum on the excitation wavelength). Instead, the electronic lines in both the LT absorption and emission spectra are notably broadened and their peak positions take an intermediate place between those for the parent compounds. E.g., the above-mentioned $Z_0 \rightarrow Y_7$ Tm^{3+} absorption line shifts to 6123.9 cm^{-1} and its width increases to 34.8 cm^{-1} (~5 times that of Tm:Lu_2O_3). This confirms the formation of a substitutional solid-solution $(Lu_{1-x}Y_x)_2O_3$ with

Optical Materials EXPRESS

Table 4. Experimental Crystal-Field Splitting of the $^3H_6$ and $^3F_4$ Tm^{3+} Multiplets in $LuYO_3$, Y_2O_3, and Lu_2O_3 Ceramics

$E(^3H_6)$, cm^{-1}				$E(^3F_4)$, cm^{-1}			
Z_i	Y_2O_3	Lu_2O_3	$LuYO_3$	Y_j	Y_2O_3	Lu_2O_3	$LuYO_3$
Z_1	0	0	0	Y_1	5612	5608	5643
Z_2	30	35	36	Y_2	5671	5673	5674
Z_3	89	88	94	Y_3	5776	5784	5773
Z_4	217	229	221	Y_4	6004	6024	6019
Z_5	229	241	239	Y_5	6016	6037	
Z_6	338	352	347	Y_6	6099	6120	6124
Z_7	376	388	383	Y_7	6113	6134	
Z_8	432	455	449	Y_8	6142	6167	6156
Z_9	439	463		Y_9	6187	6215	6203
Z_{10}	486	508	509				
Z_{11}	503	523					
Z_{12}	732	764	747				
Z_{13}	788	828	810				

a mixture of the host-forming cations at the atomic level. The compositional disorder originates from the second coordination sphere of Tm^{3+} ions formed by different sets of Lu^{3+} and Y^{3+} cations with different ionic radii. Thus, strictly speaking, one cannot speak about a predominant substitution of the host-forming Y^{3+} or Lu^{3+} cations by the dopant Tm^{3+} ones. Table 3 presents an attempt to assign the Stark sub-levels of the Tm^{3+} ion in the $LuYO_3$ ceramic.

A similar analysis for Yb^{3+} ions in a mixed $(Lu,Sc)_2O_3$ sesquioxide crystal was performed recently in [50,51] however not going down to temperatures of about 10 K. The authors have shown a tendency for increasing the crystal-field strengths in R_2O_3 sesquioxides with decreasing the R^{3+} ionic radius (which agrees with our analysis, as $R(Y^{3+}) = 0.90$ Å and $R(Lu^{3+}) = 0.861$ Å for a VI-fold oxygen coordination). They also observed a monotonous shift of the energies of Yb^{3+} Stark sub-levels with the Lu/Sc ratio. One can expect a monotonouis variation of the barycenter multiplet energies of Tm^{3+} ions in $(Lu_{1-x}Y_x)_2O_3$ solid-solutions with changing the Lu/Y ratio.

4. Conclusion

In the present work, we tried to reveal the effect of a "mixed" host composition on the spectroscopic properties of the dopant Tm^{3+} ions using the cubic sesquioxide system (R_2O_3) and analyzing a lutetia – yttria ($LuYO_3$) transparent ceramic fabricated by HIPing. Our study evidences the formation of a substitutional sesquioxide solid-solution with a mixture of cations at the atomic level according to the following findings: (i) the dominant peak in the Raman spectrum characteristic to C-type bixbyite structure takes an intermediate position between those for the parent compounds and is notably broadened; (ii) the absorption and emission spectra of the Tm^{3+} ion exhibit significant inhomogeneous broadening; (iii) at 12 K, the absorption / emission peaks corresponding to electronic transitions are notably broadened, their positions follow the variation of the crystal-field strength in the R = Y → Lu series while no evidence of two distinct Tm^{3+} species in C_2 sites with a second coordination sphere predominantly formed by Lu^{3+} or Y^{3+} is observed.

The Tm:$LuYO_3$ ceramic benefits from inhomogeneously broadened emission related to the $^3F_4 \rightarrow {}^3H_6$ transition naturally extending above 2 µm (the limit set by the total Stark splitting

Optical Materials EXPRESS

of the Tm^{3+} ground-state, $\Delta(^3H_6) = 810\ cm^{-1}$). In addition, it exhibits a long-wave emission observed up to at least 2.35 μm. The analysis of its spectral shape reveals a phonon sideband at 2.23 μm and a part with a nearly exponential dependence at longer wavelengths. The phonon sideband is associated to the coupling of electronic transitions with the most intense Raman mode of the C-type bixbyite structure (centered at 385.4 cm^{-1} for $LuYO_3$) and the exponential part – with multiphonon-assisted (vibronic) processes. All this leads to smooth (structureless) and broad gain spectra of Tm^{3+} ions supporting the generation of ultrashort (sub-100 fs) pulses. The utilization of multiphonon-assisted emission sidebands of Tm^{3+} ions in sesquioxides may be a viable way for further pulse shortening in mode-locked lasers emitting above 2 μm.

Funding. Agence Nationale de la Recherche ANR SPLENDID2 (ANR-19-CE08-0028); "RELANCE" Chair of Excellence project funded by the Normandy Region; The research at IChHPS RAS was funded by the Russian Science Foundation (21-13-00397); National Natural Science Foundation of China (61975208, 61875199, 61905247, 52032009, 61850410533, 62075090, U21A20508); Sino-German Scientist Cooperation and Exchanges Mobility Program (M-0040).

Acknowledgment. Xavier Mateos acknowledges the Serra Húnter program.

Disclosures. The authors declare no conflicts of interest.

Data availability. Data underlying the results presented in this paper are not publicly available at this time but may be obtained from the authors upon reasonable request.

References

1. C. Kränkel, "Rare-earth-doped sesquioxides for diode-pumped high-power lasers in the 1-, 2-, and 3-μm spectral range," IEEE J. Sel. Top. Quantum Electron. **21**(1), 250–262 (2015).
2. Z. Liu, A. Ikesue, and J. Li, "Research progress and prospects of rare-earth doped sesquioxide laser ceramics," J. Eur. Ceram. Soc. **41**(7), 3895–3910 (2021).
3. P. A. Loiko, K. V. Yumashev, R. Schödel, M. Peltz, C. Liebald, X. Mateos, B. Deppe, and C. Kränkel, "Thermo-optic properties of Yb:Lu_2O_3 single crystals," Appl. Phys. B **120**(4), 601–607 (2015).
4. L. Laversenne, Y. Guyot, C. Goutaudier, M. T. Cohen-Adad, and G. Boulon, "Optimization of spectroscopic properties of Yb^{3+}-doped refractory sesquioxides: cubic Y_2O_3, Lu_2O_3 and monoclinic Gd_2O_3," Opt. Mater. **16**(4), 475–483 (2001).
5. R. P. Leavitt, J. B. Gruber, N. C. Chang, and C. A. Morrison, "Optical spectra, energy levels, and crystal-field analysis of tripositive rare-earth ions in Y_2O_3. II. Non-Kramers ions in C_2 sites," J. Chem. Phys. **76**(10), 4775–4788 (1982).
6. J. B. Gruber, R. P. Leavitt, C. A. Morrison, and N. C. Chang, "Optical spectra, energy levels, and crystal-field analysis of tripositive rare-earth ions in Y_2O_3. IV. C_{3i} sites," J. Chem. Phys. **82**(12), 5373–5378 (1985).
7. P. Loiko, P. Koopmann, X. Mateos, J. M. Serres, V. Jambunathan, A. Lucianetti, T. Mocek, M. Aguiló, F. Díaz, U. Griebner, V. Petrov, and C. Kränkel, "Highly-efficient, compact Tm^{3+}:RE_2O_3 (RE = Y, Lu, Sc) sesquioxide lasers based on thermal guiding," IEEE J. Sel. Top. Quantum Electron. **24**(5), 1–13 (2018).
8. L. Fornasiero, E. Mix, V. Peters, K. Petermann, and G. Huber, "Czochralski growth and laser parameters of RE^{3+}-doped Y_2O_3 and Sc_2O_3," Ceram. Int. **26**(6), 589–592 (2000).
9. C. Goutaudier, F. S. Ermeneux, M. T. Cohen-Adad, and R. Moncorge, "Growth of pure and RE^{3+}-doped Y_2O_3 single crystals by LHPG technique," J. Cryst. Growth **210**(4), 693–698 (2000).
10. A. Ikesue and Y. L. Aung, "Ceramic laser materials," Nat. Photonics **2**(12), 721–727 (2008).
11. J. Lu, K. Takaichi, T. Uematsu, A. Shirakawa, M. Musha, K. I. Ueda, H. Yagi, T. Yanagitani, and A. A. Kaminskii, "Yb^{3+}:Y_2O_3 ceramics–a novel solid-state laser material," Jpn. J. Appl. Phys. **41**(Part 2, No. 12A), L1373–L1375 (2002).
12. P. A. Ryabochkina, A. N. Chabushkin, Y. L. Kopylov, V. V. Balashov, and K. V. Lopukhin, "Two-micron lasing in diode-pumped ceramics," Quantum Electron. **46**(7), 597–600 (2016).
13. K. Takaichi, H. Yagi, A. Shirakawa, K. Ueda, S. Hosokawa, T. Yanagitani, and A. A. Kaminskii, "Lu_2O_3:Yb^{3+} ceramics–a novel gain material for high-power solid-state lasers," Phys. Status Solidi A **202**(1), R1–R3 (2005).
14. O. L. Antipov, A. A. Novikov, N. G. Zakharov, and A. P. Zinov'ev, "Optical properties and efficient laser oscillation at 2066nm of novel Tm:Lu_2O_3 ceramics," Opt. Mater. Express **2**(2), 183–189 (2012).
15. J. Lu, J. F. Bisson, K. Takaichi, T. Uematsu, A. Shirakawa, M. Musha, K. Ueda, H. Yagi, T. Yanagitani, and A. A. Kaminskii, "Yb^{3+}:Sc_2O_3 ceramic laser," Appl. Phys. Lett. **83**(6), 1101–1103 (2003).
16. W. Jing, P. Loiko, J. Maria Serres, Y. Wang, E. Vilejshikova, M. Aguiló, F. Díaz, U. Griebner, H. Huang, V. Petrov, and X. Mateos, "Synthesis, spectroscopy, and efficient laser operation of "mixed" sesquioxide Tm:$(Lu,Sc)_2O_3$ transparent ceramics," Opt. Mater. Express **7**(11), 4192–4202 (2017).
17. J. Saikawa, Y. Sato, T. Taira, and A. Ikesue, "Passive mode locking of a mixed garnet Yb:$Y_3ScAl_4O_{12}$ ceramic laser," Appl. Phys. Lett. **85**(24), 5845–5847 (2004).
18. A. Pirri, B. Patrizi, R. N. Maksimov, V. A. Shitov, V. V. Osipov, M. Vannini, and G. Toci, "Spectroscopic investigation and laser behaviour of Yb-doped laser ceramics based on mixed crystalline structure $(Sc_xY_{1-x})_2O_3$," Ceram. Int. **47**(20), 29483–29489 (2021).

Optical Materials EXPRESS

19. A. Schmidt, V. Petrov, U. Griebner, R. Peters, K. Petermann, G. Huber, C. Fiebig, K. Paschke, and G. Erbert, "Diode-pumped mode-locked Yb:$LuScO_3$ single crystal laser with 74 fs pulse duration," Opt. Lett. **35**(4), 511–513 (2010).
20. C. Kränkel, A. Uvarova, É Haurat, L. Hülshoff, M. Brützam, C. Guguschev, S. Kalusniak, and D. Klimm, "Czochralski growth of mixed cubic sesquioxide crystals in the ternary system Lu_2O_3–Sc_2O_3–Y_2O_3," Acta Crystallogr., Sect. B: Struct. Sci., Cryst. Eng. Mater. **77**(4), 550–558 (2021).
21. W. Jing, P. Loiko, J. M. Serres, Y. Wang, E. Kifle, E. Vilejshikova, M. Aguiló, F. Díaz, U. Griebner, H. Huang, and V. Petrov, "Synthesis, spectroscopic characterization and laser operation of Ho^{3+} in "mixed" (Lu,Sc)2O3 ceramics," J. Lumin. **203**, 145–151 (2018).
22. L. Basyrova, P. Loiko, W. Jing, Y. Wang, H. Huang, E. Dunina, A. Kornienko, L. Fomicheva, B. Viana, U. Griebner, V. Petrov, M. Aguiló, F. Díaz, X. Mateos, and P. Camy, "Spectroscopy and efficient laser operation around 2.8 µm of Er:$(Lu,Sc)_2O_3$ sesquioxide ceramics," J. Lumin. **240**, 118373 (2021).
23. X. Xu, Z. Hu, D. Li, P. Liu, J. Zhang, B. Xu, and J. Xu, "First laser oscillation of diode-pumped Tm^{3+}-doped $LuScO_3$ mixed sesquioxide ceramic," Opt. Express **25**(13), 15322–15329 (2017).
24. Z. Hao, L. Zhang, Y. Wang, H. Wu, G. H. Pan, H. Wu, X. Zhang, D. Zhao, and J. Zhang, "11 W continuous-wave laser operation at 2.09 µm in Tm:$Lu_{1.6}Sc_{0.4}O_3$ mixed sesquioxide ceramics pumped by a 796 nm laser diode," Opt. Mater. Express **8**(11), 3615–3621 (2018).
25. W. Jing, P. Loiko, L. Basyrova, Y. Wang, H. Huang, P. Camy, U. Griebner, V. Petrov, J. M. Serres, R. M. Solé, M. Aguiló, F. Díazd, and X. Mateos, "Spectroscopy and laser operation of highly-doped 10 at.% Yb:$(Lu,Sc)_2O_3$ ceramics," Opt. Mater. **117**, 111128 (2021).
26. P. Koopmann, S. Lamrini, K. Scholle, P. Fuhrberg, K. Petermann, and G. Huber, "Efficient diode-pumped laser operation of Tm:Lu_2O_3 around 2 µm," Opt. Lett. **36**(6), 948–950 (2011).
27. A. Suzuki, C. Kränkel, and M. Tokurakawa, "High quality-factor Kerr-lens mode-locked Tm:Sc_2O_3 single crystal laser with anomalous spectral broadening," Appl. Phys. Express **13**(5), 052007 (2020).
28. Y. Wang, W. Jing, P. Loiko, Y. Zhao, H. Huang, X. Mateos, S. Suomalainen, A. Härkönen, M. Guina, U. Griebner, and V. Petrov, "Sub-10 optical-cycle passively mode-locked Tm:$(Lu_{2/3}Sc_{1/3})_2O_3$ ceramic laser at 2 µm," Opt. Express **26**(8), 10299–10304 (2018).
29. Y. Zhao, L. Wang, W. Chen, Z. Pan, Y. Wang, P. Liu, X. Xu, Y. Liu, D. Shen, J. Zhang, M. Guina, X. Mateos, P. Loiko, Z. Wang, X. Xu, J. Xu, M. Mero, U. Griebner, and V. Petrov, "SESAM mode-locked Tm:$LuYO_3$ ceramic laser generating 54-fs pulses at 2048 nm," Appl. Opt. **59**(33), 10493–10497 (2020).
30. Y. Zhao, L. Wang, Y. Wang, J. Zhang, P. Liu, X. Xu, Y. Liu, D. Shen, J. E. Bae, T. G. Park, F. Rotermund, X. Mateos, P. Loiko, Z. Wang, X. Xu, J. Xu, M. Mero, U. Griebner, V. Petrov, and W. Chen, "SWCNT-SA mode-locked Tm:$LuYO_3$ ceramic laser delivering 8-optical-cycle pulses at 2.05 µm," Opt. Lett. **45**(2), 459–462 (2020).
31. Y. Repelin, C. Proust, E. Husson, and J. M. Beny, "Vibrational spectroscopy of the C-form of yttrium sesquioxide," J. Solid State Chem. **118**(1), 163–169 (1995).
32. N. D. Todorov, M. V. Abrashev, V. Marinova, M. Kadiyski, L. Dimowa, and E. Faulques, "Raman spectroscopy and lattice dynamical calculations of Sc_2O_3 single crystals," Phys. Rev. B **87**(10), 104301 (2013).
33. D. E. Zelmon, J. M. Northridge, N. D. Haynes, D. Perlov, and K. Petermann, "Temperature-dependent Sellmeier equations for rare-earth sesquioxides," Appl. Opt. **52**(16), 3824–3828 (2013).
34. D. Zhang, W. Lin, Z. Lin, L. Jia, W. Zheng, and F. Huang, "Lu_2O_3: A promising ultrawide bandgap semiconductor for deep UV photodetector," Appl. Phys. Lett. **118**(21), 211906–4 (2021).
35. B. R. Judd, "Optical absorption intensities of rare-earth ions," Phys. Rev. **127**(3), 750–761 (1962).
36. G. S. Ofelt, "Intensities of crystal spectra of rare-earth ions," J. Chem. Phys. **37**(3), 511–520 (1962).
37. A. A. Kornienko and E. B. Dunina, "Determination of intensity parameters from the fine details of the Stark structure in the energy spectrum of Tm^{3+} ions in $Y_3Al_5O_{12}$," Opt. Spectrosc. **97**(1), 68–75 (2004).
38. L. Zhang, H. Lin, G. Zhang, X. Mateos, J. Maria Serres, M. Aguiló, F. Díaz, U. Griebner, V. Petrov, Y. Wang, P. Loiko, E. Vilejshikova, K. Yumashev, Z. Lin, and W. Chen, "Crystal growth, optical spectroscopy and laser action of Tm^{3+}-doped monoclinic magnesium tungstate," Opt. Express **25**(4), 3682–3693 (2017).
39. R. Moncorgé, Y. Guyot, C. Kränkel, K. Lebbou, and A. Yoshikawa, "Mid-infrared emission properties of the Tm^{3+}-doped sesquioxide crystals Y_2O_3, Lu_2O_3, Sc_2O_3 and mixed compounds $(Y,Lu,Sc)_2O_3$ around 1.5-, 2-and 2.3-µm," J. Lumin. **241**, 118537 (2022).
40. L. Guillemot, P. Loiko, R. Soulard, A. Braud, J. L. Doualan, A. Hideur, and P. Camy, "Close look on cubic Tm:KY_3F_{10} crystal for highly efficient lasing on the $^3H_4 \rightarrow {}^3H_5$ transition," Opt. Express **28**(3), 3451–3463 (2020).
41. P. Loiko, E. Kifle, L. Guillemot, J. L. Doualan, F. Starecki, A. Braud, M. Aguiló, F. Díaz, V. Petrov, X. Mateos, and P. Camy, "Highly efficient 2.3 µm thulium lasers based on a high-phonon-energy crystal: evidence of vibronic-assisted emissions," J. Opt. Soc. Am. B **38**(2), 482–495 (2021).
42. S. Tanabe, K. Hirao, and N. Soga, "Local structure of rare-earth ions in fluorophosphate glasses by phonon sideband and Mössbauer spectroscopy," J. Non-Cryst. Solids **142**, 148–154 (1992).
43. F. Auzel, "Multiphonon-assisted anti-Stokes and Stokes fluorescence of triply ionized rare-earth ions," Phys. Rev. B **13**(7), 2809–2817 (1976).
44. P. Loiko, X. Mateos, S. Y. Choi, F. Rotermund, J. M. Serres, M. Aguiló, F. Díaz, K. Yumashev, U. Griebner, and V. Petrov, "Vibronic thulium laser at 2131 nm Q-switched by single-walled carbon nanotubes," J. Opt. Soc. Am. B **33**(11), D19–D27 (2016).

Optical Materials EXPRESS

45. S. A. Payne, L. L. Chase, L. K. Smith, W. L. Kway, and W. F. Krupke, "Infrared cross-section measurements for crystals doped with Er^{3+}, Tm^{3+} and Ho^{3+}," IEEE J. Quantum Electron. **28**(11), 2619–2630 (1992).
46. B. F. Aull and H. P. Jenssen, "Vibronic interactions in Nd:YAG resulting in nonreciprocity of absorption and stimulated emission cross sections," IEEE J. Quantum Electron. **18**(5), 925–930 (1982).
47. Y. Zhao, L. Wang, W. Chen, P. Loiko, Y. Wang, Z. Pan, H. Yang, W. Jing, H. Huang, J. Liu, X. Mateos, Z. Wang, X. Xu, U. Griebner, and V. Petrov, "Kerr-lens mode-locked Tm-doped sesquioxide ceramic laser," Opt. Lett. **46**(14), 3428–3431 (2021).
48. P. Loiko and M. Pollnau, "Stochastic model of energy-transfer processes among rare-earth ions. Example of Al_2O_3:Tm^{3+}," J. Phys. Chem. C **120**(46), 26480–26489 (2016).
49. A. Lupei, V. Lupei, S. Grecu, C. Tiseanu, and G. Boulon, "Crystal-field levels of Tm^{3+} in gadolinium gallium garnet," J. Appl. Phys. **75**(9), 4652–4657 (1994).
50. W. Liu, D. Lu, S. Pan, M. Xu, Y. Hang, H. Yu, H. Zhang, and J. Wang, "Ligand engineering for broadening infrared luminescence of Kramers ytterbium ions in disordered sesquioxides," Cryst. Growth Des. **19**(7), 3704–3713 (2019).
51. R. Guo, D. Huang, D. Lu, F. Liang, Q. Zhang, H. Yu, and H. Zhang, "Spectral broadening mechanism of Yb^{3+}-doped cubic $Lu_xSc_{2-x}O_3$ sesquioxide crystals for ultrafast lasers," Opt. Mater. Express **12**(5), 1963–1976 (2022).